Pergamon

0301-9322(95)00006-2

Int. J. Multiphase Flow Vol. 21, No. 4, pp. 561–567, 1995

0301-9322/95 $9.50 + 0.00

NUMERICAL SIMULATION OF THE TICKING HOURGLASS†

E. MANGER[1], T. SOLBERG[1], B. H. HJERTAGER[1] and D. VAREIDE[2]

[1]Telemark Institute of Technology and Telemark Technological R & D Centre, N-3914 Porsgrunn, Norway

[2]Statoil Research Centre, Postuttak, N-7005 Trondheim, Norway

(Received 22 September 1994; in revised form 22 January 1995)

Abstract—Using a two-phase fluid flow model based on kinetic theory for granular flow the oscillatory flow of sand in an hourglass first observed experimentally by Wu *et al.* has been simulated. The oscillations appear to be caused by the interaction between the gas pressure and the flow of sand through the orifice of the hourglass. The simulations confirm the ticking of the hourglass and the suggested mechanisms for this behaviour found experimentally by Wu *et al.* The simulations also show bubbles of air rising through the powder as observed experimentally.

Key Words: ticking hourglass, curvilinear co-ordinates, kinetic theory, fluidized flow, oscillatory flow

INTRODUCTION

The flow in hourglasses made for commercial use is normally steady. Recently, a new surprising effect has been observed by Wu *et al.* (1993). When the particle diameter of the solid is small, $d_p \sim 10$–$100\ \mu$m, the flow of solid is only steady in the narrow range $2 < D/d_p < 12$, where D is the diameter of the orifice. For $D/d_p > 12$, the flow is intermittent with a well-defined frequency of oscillations.

This paper presents simulations of this particular phenomena. We use a two-phase fluid model for space sharing interspersed continua to describe the system. Kinetic theory for granular flow (Gidaspow 1994) is used to determine the fluctuations in the particle phase. Likewise, the solid phase pressure, bulk viscosity and shear viscosity are deduced from this theory.

First we give a brief overview of the governing equations and the numerical solution procedure. Then, the numerical results are presented. Finally, the validity of the numerical results is discussed, and conclusions are drawn.

GOVERNING EQUATIONS

Using physical covariant velocity projections, the conservation laws governing the two-phase air–particle flow (Gidaspow 1994) are formulated in general curvilinear co-ordinates.

The continuity equations read

$$\frac{\partial}{\partial t}(\epsilon\rho)_n + \frac{\Delta}{\Delta\xi^i}(g^{im}\epsilon\rho U_m)_n = 0$$

where $n = $ G (gas) or s (solid). Here ϵ denotes the volume fraction and ρ is the density of phase n. U_m is the m-component of the physical, covariant velocity projection and g^{im} is the contravariant metric tensor component. $\Delta/\Delta\xi^i$ denotes the divergence in the curvilinear co-ordinate system.

Likewise, the momentum equations are given by

$$\frac{\partial}{\partial t}(\epsilon_\rho U_j)_n + \frac{\Delta}{\Delta\xi^i}(g^{im}\epsilon\rho U_m U_j)_n = -\epsilon_n\frac{\partial p}{\partial\xi^j} + \frac{\Delta}{\Delta\xi^i}(\tau_{ij})_n + (\epsilon\rho)_n b_j + \beta_j[(U_j)_N - (U_j)_n]$$

where p is the pressure, $\partial/\partial\xi^j$ is the partial derivative with respect to ξ^i, b_j is the j-component of the body force and β_j is the j-component of the two-phase drag coefficient.

†This paper was presented at the *7th Israeli–Norwegian Scientific Symposium on Fluid Mechanics of Heterogeneous Systems*, 20–22 June 1994, Trondheim, Norway.

The stress tensor τ_{ij} for the gas phase is expressed as

$$(\tau_{ij})_G = \mu_{a,l}\left[\left(\frac{\partial U_j}{\partial \xi^i} + \frac{\partial U_i}{\partial \xi^j}\right)_G - \tfrac{2}{3}\delta_{ij}\frac{\Delta}{\Delta \xi^l}(g^{lm}U_m)_G\right]$$

and for the solid phase as

$$(\tau_{ij})_s = -P_s\delta_{ij} + \zeta_s\delta_{ij}\frac{\Delta}{\Delta \xi_l}(g^{lm}U_m)_s + \mu_s\left[\left(\frac{\partial U_j}{\partial \xi^i} + \frac{\partial U_i}{\partial \xi^j}\right)_s - \tfrac{2}{3}\delta_{ij}\frac{\Delta}{\Delta \xi_l}(g^{lm}U_m)_s\right]$$

Here $\mu_{G,l}$ is the laminar gas viscosity and δ_{ij} is the Kroenecker delta. The solid phase pressure P_s, bulk viscosity ζ_s and shear viscosity μ_s are derived from kinetic theory for granular flow, giving the following expressions:

$$P_s = \epsilon_s\rho_s(1 + 2(1+e)\epsilon_s g_0)\Theta$$

$$\zeta_s = \tfrac{4}{3}\epsilon_s^2\rho_s d_p g_0(1+e)\sqrt{\frac{\Theta}{\pi}}$$

$$\mu_s = \frac{2\mu_{s,dil}}{(1+e)g_0}[1 + \tfrac{4}{5}(1+e)g_0\epsilon_s]^2 + \tfrac{4}{5}\epsilon_s^2\rho_s d_p g_0(1+e)\sqrt{\frac{\Theta}{\pi}}$$

Here e is the restitution coefficient and Θ is the turbulent kinetic energy for the solid phase. The dilute part of the shear viscosity $\mu_{s,dil}$ and the radial distribution function g_0 are given by

$$\mu_{s,dil} = \tfrac{5}{96}\rho_s d_p\sqrt{\pi\Theta}$$

$$g_0 = \frac{3}{5}\left[1 - \left(\frac{\epsilon_s}{\epsilon_{s,max}}\right)^{1/3}\right]^{-1}$$

where $\epsilon_{s,max}$ is the maximum packing of solids, assumed here to be 0.65.

Again from kinetic theory for granular flow, the turbulent kinetic energy Θ of the solid phase is governed by the transport equation

$$\frac{3}{2}\left[\frac{\partial}{\partial t}(\epsilon\rho\Theta)_s + \frac{\Delta}{\Delta \xi^i}(g^{im}\epsilon\rho U_m\Theta)_s\right] = (\tau_{ij})_s\frac{\Delta}{\Delta \xi^i}(g^{jm}U_m)_s + \frac{\Delta}{\Delta \xi^i}\left[g^{ik}\Gamma_\Theta\frac{\Delta\Theta}{\Delta \xi^k}\right] - \gamma$$

The dissipation γ in this equation, found from kinetic theory, is given by an algebraic expression

$$\gamma = 3(1-e^2)\epsilon_s^2\rho_s g_0\Theta\left[\frac{4}{d_p}\sqrt{\frac{\Theta}{\pi}} - \frac{\Delta}{\Delta \xi^i}(g^{il}U_l)_s\right]$$

The transport coefficient has the form

$$\Gamma_\Theta = \frac{2\Gamma_{\Theta,dil}}{(1+e)g_0}[1 + \tfrac{6}{5}(1+e)g_0\epsilon_s]^2 + 2\epsilon_s^2\rho_s d_p g_0(1+e)\sqrt{\frac{\Theta}{\pi}}$$

where

$$\Gamma_{\Theta,dil} = \tfrac{75}{384}\rho_s d_p\sqrt{\pi\Theta}$$

Finally, the drag expressions must be formulated. For $\epsilon_G \leqslant 0.8$, the drag is based on the Ergun equation giving

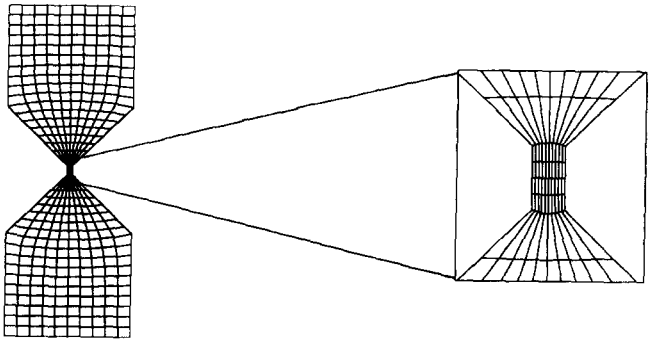

Figure 1. Grid used in the simulations.

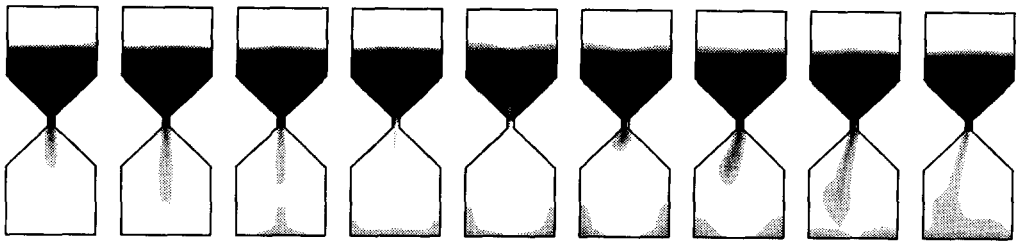

Figure 2. Void fraction of powder at different times, $t_0 = 1.0$ s and $\Delta t = 0.4$ s.

$$\beta = 150\frac{\epsilon_s^2 \mu_{G,l}}{\epsilon_G (d_p \Phi_s)^2} + 1.75\frac{\epsilon_s \rho_G |\mathbf{U}_G - \mathbf{U}_s|}{d_p \Phi_s}$$

and for $\epsilon_G > 0.8$, the drag is based on the single sphere drag resulting in

$$\beta = \tfrac{3}{4} C_d \frac{|\mathbf{U}_G - \mathbf{U}_s| \rho_G \epsilon_G \epsilon_s}{d_p \Phi_s} \epsilon_G^{-2.65}$$

where Φ_s is the form factor for the particles. The drag coefficient is given by

$$C_d = \frac{24}{\mathrm{Re}}(1 + 0.15\,\mathrm{Re}^{0.687}) \quad \text{for } \mathrm{Re} \leqslant 1000$$

$$C_d = 0.44 \quad \text{for } \mathrm{Re} > 1000$$

and the Reynolds number for particulate flow is defined as

$$\mathrm{Re} = \frac{|\mathbf{U}_G - \mathbf{U}_s| \epsilon_G \rho_G d_p}{\mu_{G,l}}$$

Only a brief description of the model is given above. A more comprehensive description can be found in Gidaspow (1994).

SOLUTION PROCEDURE

The governing equations are solved by a finite volume method (Patankar 1980). The calculation domain is divided into a finite number of control volumes, and the grid points are defined such that each grid point is surrounded by a control volume. By integrating the conservation equations in space and time, the set of differential equations transform to a set of algebraic difference equations for each control volume. Upwind spatial differencing and fully implicit Euler temporal

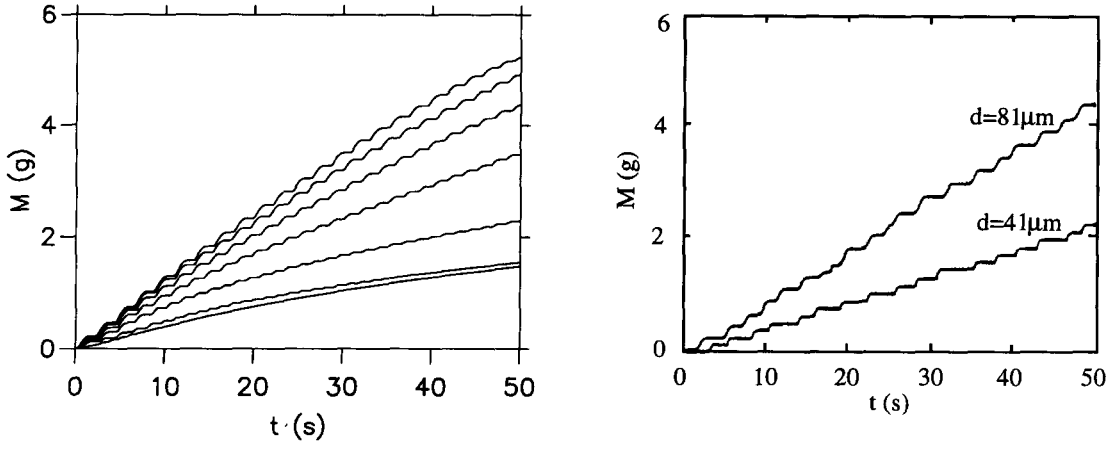

Figure 3. The total mass flow through the hourglass. The simulation results are shown to the left, and the experimental results to the right. The simulations show larger mass transport for larger particle diameter, with particle diameters between 20 and 127 μm.

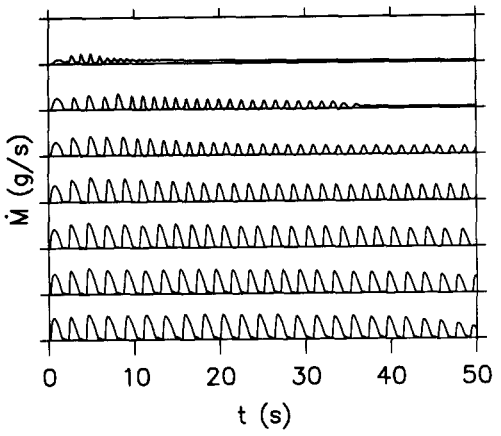

Figure 4. The mass flux through the orifice of the hourglass for various particle diameters. The largest particle diameter is shown at the top with decreasing particle diameter downwards.

differencing are adopted. The discretization procedure based on a staggered grid follows that of Karki & Patankar (1988) for general non-orthogonal co-ordinates.

Because of the strong coupling between the phases through the drag forces, a PEA-algorithm (partial elimination algorithm) (Spalding 1985) is introduced to decouple the momentum equations. The coupling between the continuity and the momentum equations is taken care of by the SIMPLE-algorithm (semi-implicit method for pressure linked equations) (Patankar 1980).

NUMERICAL RESULTS

Figure 1 shows the hourglass along with the curvilinear grid used in the simulations. The diameter of the orifice of the hourglass is 0.2 cm. Although the hourglass is axisymmetric, the present study is limited to a planar geometry. Still, the qualitative properties should be maintained. The main issue of this study will therefore be to demonstrate the qualitative behaviour of the model rather than to achieve perfect agreement between simulation results and experimental results.

Figure 2 shows the void fraction of powder at time intervals of 0.4 s, starting at $t = 1.0$ s with particle diameter $d_p = 81$ μm. The simulation clearly shows that the powder flow is discontinuous. This is related to the gas bubble which is formed in the solid phase when the flow of particles through the orifice is zero. The bubble rises upwards through the powder and breaks at the powder surface. Such bubbles have been observed experimentally by Wu *et al.* (1993).

In order to verify the two-phase particulate flow modelling based on kinetic theory for granular flow, simulations with six different particle sizes are performed. The chosen particle diameters are

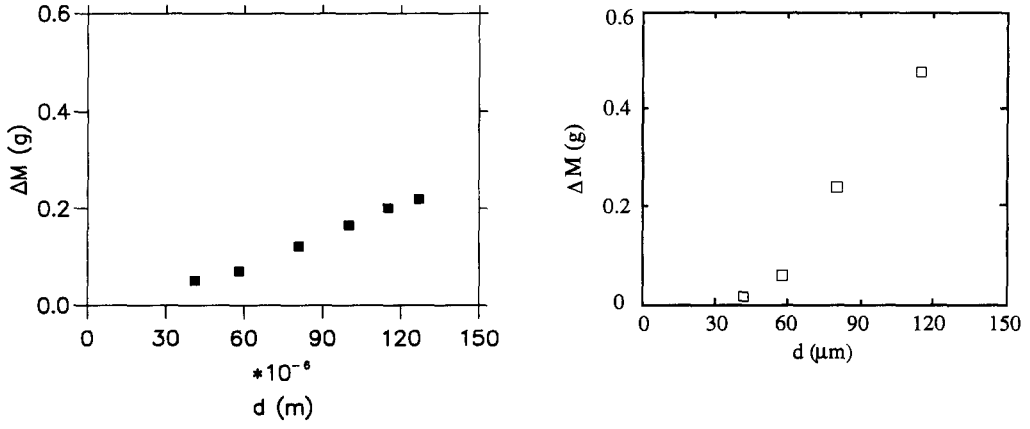

Figure 5. The average mass transfer per avalanche for various particle diameters. The simulation results are again shown in the left figure.

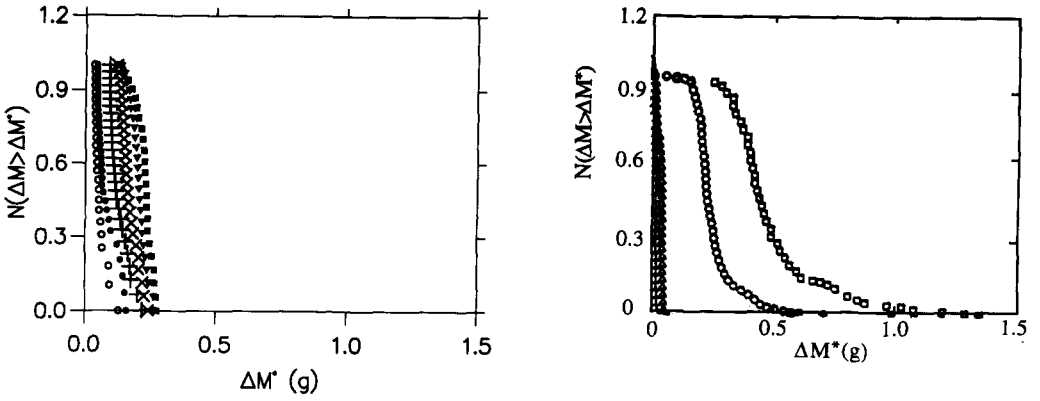

Figure 6. The cumulative mass distribution $N(\Delta M > \Delta M^*)$ found from simulations and from experiments with experimental results shown to the right. The markers are for the following sizes: 0.41 μm (○), 58 μm (●), 81 μm (+), 100 μm (×), 115 μm (■) and 127 μm (▼).

20, 41, 58, 81, 100, 115 and 127 μm, covering the range $16 \leqslant D/d_p \leqslant 100$. The experimental investigations of Wu *et al.* (1993) were carried out with the particle diameters 41, 58, 81, 115 and 168 μm.

In the following section, the numerical results are compared with the experimental results of Wu *et al.* (1993). In the figures, the numerical results are shown to the left and the experimental results to the right.

Figure 3 shows the simulated total mass through the orifice compared with the experimental results. The simulations and the experimental results show qualitatively similar oscillatory flow.

The flux through the orifice of the hourglass is shown in figure 4 as a function of time. This figure shows how the transport through the orifice oscillates with time. An intermittent flow is obtained with a well defined period of oscillations. The figure also shows that for $D/d_p \geqslant 49$ ($d_p \leqslant 41$ μm), the oscillations decay and eventually the flow through the orifice becomes steady.

The average mass transfer per avalanche, ΔM, is shown for various particle diameters in figure 5. Simulations show that ΔM increases with increasing particle diameter as found experimentally. There is, however, some discrepancy in the values, and note that this discrepancy increases with larger particle sizes. A general trend for the simulations is that larger particle sizes result in larger deviations from measurements.

Figure 6 shows the cumulative mass distribution $N(\Delta M > \Delta M^*)$. The simulations give reasonable agreement with experimental results for small particle diameters, but the discrepancy increases as the particle size grows. Again, the numerical results follow the general trend mentioned earlier. For large particle diameters, the simulated throughput of the orifice is much too low.

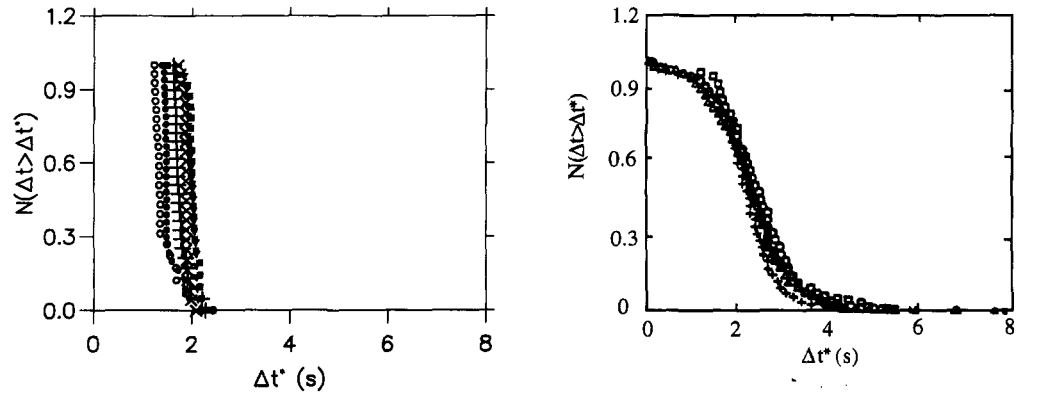

Figure 7. The cumulative time distribution $N(\Delta t > \Delta t^*)$ found from simulations and from experiments with experimental results to the right. The markers are the same as in the previous figure.

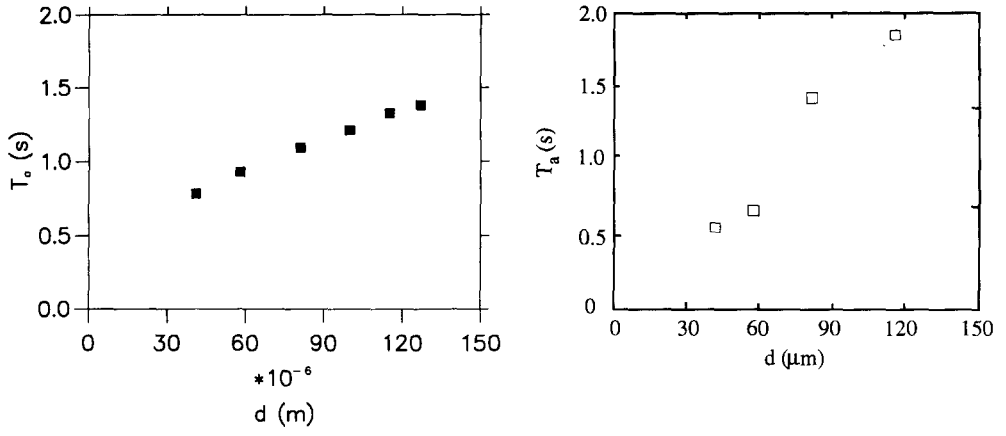

Figure 8. The time interval of the active period in the oscillations for different particle diameters. Simulation results are shown in the left figure.

The results above have, by means of theory, shown that the hourglass will tick. There will be an active phase with time interval T_a, where the sand flows through the orifice of the hourglass, and there will be an inactive phase where there is no flow through the orifice. The total period of the oscillations, T, is defined (Wu *et al.* 1993) as the sum of time intervals for these two phases for one avalanche.

The cumulative time distribution for the total period T is shown in figure 7. The simulations give a much sharper distribution compared to the experimental results. However, the general distribution function for the simulations agrees well with the corresponding experimental function with approximately the same average value.

Figure 8 shows the average time interval of the active phase defined above. As demonstrated earlier, there is good agreement when the particle size is small, but the discrepancy increases with increasing particle diameter.

DISCUSSION AND CONCLUSIONS

The flow of sand in an hourglass has been simulated using a two-phase flow model based on kinetic theory for granular flow. The simulations show qualitative agreement with the experimental findings of Wu *et al.* (1993). Like the measurements, the simulations indicate an oscillatory flow of sand through the orifice of the hourglass with a well defined period of oscillations for the diameter of the orifice to the particle diameter ratio $D/d_p \geqslant 16$. Both experiments and simulations indicate that the oscillatory flow is induced by a gas bubble which is formed in the solid phase at the orifice. The bubble rises through the sand and breaks at the surface. Unlike the experiments, the simulations indicate that the flow of sand through the orifice is steady for a ratio $D/d_p \geqslant 49$.

Quantitative comparisons with the measurements of Wu *et al.* (1993) show significant deviations in the simulations. Part of the discrepancies may be explained by limitations in the physical model as well as the numerical differencing scheme. First of all, the simulations are limited to a planar geometry whereas the experimental hourglass is axisymmetric. Furthermore, the two-phase flow model is based on a continuum approach. As the ratio D/d_p becomes smaller, the flow of sand through the orifice can eventually not be treated as a continuum any longer. Likewise, the two-phase model is based on fluidization of the solid phase. Only the flow of sand just above and through the orifice can, however, be characterized as being fluidized. Finally, the numerical differencing scheme is not optimal. A numerical scheme based on fully implicit Euler temporal and upwind spatial differencing is well known to produce artificial damping or smearing.

Acknowledgements—The present work was supported by the Research Council of Norway (NFR) through the SMOGASOL program (simulation, measurement, monitoring and control of gas/solids systems in the process industry). The authors are grateful to the Statoil Research Centre for financial support to publish these results.

REFERENCES

Gidaspow, D. 1994 *Multiphase Flow and Fluidization, Continuum and Kinetic Theory Descriptions.* Academic Press, New York.

Karki, K. C. & Patankar, S. V. 1988 Calculation procedure for viscous incompressible flows in complex geometries. *Numer. Heat Transfer* **14,** 295–307.

Patankar, S. V. 1980 *Numerical Heat Transfer and Fluid Flow.* Hemisphere, Washington DC.

Spalding, D. B. 1985 Computer simulation of two-phase flows with special reference to nuclear reactor systems. In *Computational Techniques in Heat Transfer,* pp. 1–44. Pineridge Press.

Wu, X.-L., Måløy, K. J., Hansen, A., Ammi, M. & Bideau, D. 1993 Why hour glasses tick. *Phys. Rev. Lett.* **71,** 1363–1366.